Jurnal Teknologi

Full Paper

THE EFFECT OF CRYSTALLIZATION AND AGING TIME IN ZEOLITE SYNTHESIS USING COAL FLY ASH AS SILICA AND ALUMINA SOURCE

Abdul Aziz[a], Rahmi[a], Lenny Marlinda[b*]

[a]Department of Chemistry, University of Jambi, Jambi, 36361, Indonesia
[b]Department of Industrial Chemistry, University of Jambi, Jambi, 36361, Indonesia

Article history
Received
29 February 2024
Received in revised form
18 October 2024
Accepted
12 November 2024
Published Online
28 April 2025

*Corresponding author
marlindalenny@unja.ac.id

Graphical abstract

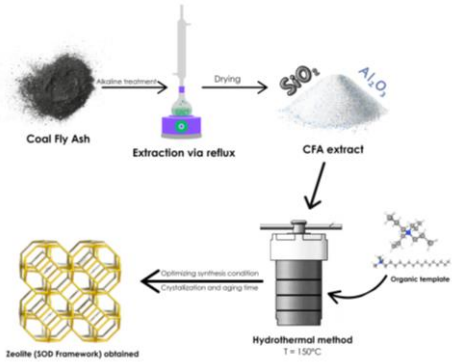

Abstract

Silica and alumina were extracted from coal fly ash (CFA) using a reflux method with an alkaline solution. The resulting coal fly ash extract (CFAE) served as the primary material for synthesizing zeolites through a hydrothermal method at 150°C, with variations in crystallization time (ranging from 10 to 120 hours) and aging time (ranging from 0 to 24 hours). Hence, this study aims to utilize CFA waste to synthesize zeolite without adding external silica and alumina while evaluating the optimal crystallization and aging time synthesis conditions using the hydrothermal method. XRF characterization revealed increased alumina and silica composition in CFAE, from 16.7669% and 30.8462% to 42.04% and 53.42%, respectively. Analysis of FTIR spectra showed characteristic absorptions indicative of zeolite structures, while XRD data analysis confirmed the presence of zeolite ZK-14 (SOD) phase in all synthesized samples. The %yield, crystallinity, and particle size of the synthesized materials were significantly influenced by variations in crystallization and aging times. %Yield showed slight variation, with the highest achieved at 48 hours of crystallization time (37.83%). Crystallinity increased with prolonged crystallization time, peaking at 72 hours (50.73%), while particle size reached its maximum at 120 hours (23.82 nm). Aging time exhibited an inverse relationship with crystallinity and particle size but did not affect %yield. Overall, longer crystallization times led to higher %yield, crystallinity, and larger particle size in the synthesized zeolite materials.

Keywords: Aging time, coal fly ash, crystallization time, silica and alumina source, synthesis zeolite

1.0 INTRODUCTION

Coal fly ash (CFA) is a byproduct of coal combustion generated in every Coal-Fired Power Plant. CFA is considered hazardous waste that can pollute the environment if released without proper handling. It contains heavy metals such as Pb, Cd, Cr, Co, Cu, and others, contaminating the soil, water, and air and posing risks to human health through the food chain. There is a possibility that fly ash may contain heavy metals up to 10 times more than coal itself [1].

According to Luo and colleagues [2], the composition of fly ash in bituminous coal is predominantly composed of SiO_2, ranging from approximately 20-60 wt%, and Al_2O_3, approximately 5-35 wt%, along with various metal oxides such as Fe_2O_3, CaO, MgO, Na_2O, SO_3, and other metal oxides. Direct utilization of CFA is commonly employed in the construction industry to produce cement and concrete, including bricks and blocks. Additionally, it serves as an additional functional material for synthesizing geopolymers and zeolites. On

the other hand, indirect utilization tends to focus on extracting valuable elements or compounds present in CFA through metallurgical processes such as the separation of magnetite, alumina, and titanium fractions [3].

In a study by Ndlovu [4], silica and alumina were successfully extracted from CFA and subsequently utilized in synthesizing zeolite ZSM-5, faujasite, and geopolymers. The process began by extracting alumina using concentrated H_2SO_4 in a digestion vessel. The residue obtained from the alumina extraction was then subjected to further extraction of the remaining silica using a reflux system with NaOH solvent. This extraction process successfully yielded 88.03% alumina and 85.74% silica. Therefore, CFA holds great potential as an alternative material for zeolite synthesis.

In several studies, CFA has been utilized as an additional source of silica and alumina for synthesizing zeolite under various conditions. Various methods have been employed for zeolite synthesis, including the sol-gel method [5, 6], co-precipitation [7], microwave-assisted [8, 9], and hydrothermal methods [10,11,8,12,13]. The hydrothermal method is the most widely used among these methods and remains prevalent to date. Its advantages include reducing particle agglomeration, producing relatively uniform crystal sizes, and generating homogeneous crystals at relatively low temperatures (below 150°C). Additionally, the hydrothermal method is favored for its cost-effectiveness, mass efficiency, high purity of the resulting products, easy reaction control based on stoichiometric ratios, scalability to industrial levels, environmental friendliness, and sufficient accessibility for controlling complex size distribution, shape, and chemical composition [14].

Various types of zeolites have been successfully synthesized using CFA as a source of silica and alumina without the addition of pure alumina and silica. Typically, the zeolite types formed have an intermediate silica (Si/Al ratio of 2-5), such as zeolites with CHA, FAU, and SOD framework structures [15]. In a study conducted by Aldahri and colleagues [16], zeolites were synthesized from CFA as a source of alumina and silica using a simple hydrothermal method. The resulting zeolite was identified as Na-P zeolite with an SOD framework structure. Similar results were obtained by Liu and colleagues [17], who synthesized zeolites from CFA as a source of alumina and silica using a hydrothermal method. The zeolites obtained were Na-P zeolite (GIS), sodalite, and zeolite-X, all of which had SOD framework structures.

Several factors, including the use of structure-directing templates, aging time, and crystallization time, influence the synthesis process of zeolite. Structure-directing templates play a crucial role in directing the pore size of the synthesized zeolite structure. Commonly used organic templates include tetrapropylammonium hydroxide (TPAOH) and tetrapropylammonium bromide (TPABr) as micro-pore structure directors [18] and Cetyltrimethylammonium bromide (CTAB) as a meso-pore structure director [19]. Aging time also affects the formation of zeolite crystallites. During the aging process, the formation of primary zeolite precursors occurs. The longer the aging time, the greater the number of primary zeolite precursors formed, leading to increased aggregates transforming into larger particles [20].

Hydrothermal time also influences the structure formed, including surface area, crystal size, and crystallinity. Longer crystallization times enhance crystallinity by increasing nucleation and crystal growth rates. This, in turn, leads to improved crystallinity. Furthermore, prolonged crystallization times decrease the aluminosilicate composition [21]. Although the hydrothermal method offers several advantages, it requires an extended processing time, particularly during the crystallization and aging phases. Different materials necessitate varying durations to reach their optimal conditions. Therefore, this study will utilize CFA waste as the primary source of silica and alumina for synthesizing zeolite through the hydrothermal method, with an emphasis on determining the optimal crystallization and aging times.

2.0 METHODOLOGY

2.1 Materials

The main materials used in this study are CFA waste obtained from PT. DSSP Power Plant in South Sumatra, Indonesia. Additionally, chemicals such as 32% hydrochloric acid (HCl) from KDP, sodium hydroxide (NaOH), TPABr, CTAB, and deionized water are utilized in the research.

2.2 Coal Fly Ash Preparations (CFAP)

The CFA is homogenized by sieving it through a 200-mesh sieve. 250 grams of CFA are mixed with 500 mL of deionized water using a magnetic stirrer for 6 hours at room temperature. Subsequently, the mixture is filtered and dried at 110°C. The dried CFA is then subjected to calcination at 700°C for 3 hours.

2.3 Extraction of Silica and Alumina from Coal Fly Ash (CFAE)

The CFA extraction process follows and modifies the method conducted by Ndlovu; CFA prepared in advance is refluxed with 4M NaOH in a 1:5 ratio at 80-90°C for 4 hours. The refluxed mixture is then filtered, cooled, and the obtained filtrate undergoes pH checking. The pH is neutralized (pH 8-10) using HCl [22, 23]. The resulting precipitate or gel is allowed to stand for 3 days, followed by separation and drying at 80°C until completely dry.

2.4 Synthesis Zeolite Process

The synthesis process refers to and modifies the research conducted by Wang and colleagues [24] using a molar ratio of 40 SiO2: 20 Al_2O_3: 20 NaOH: 10

TPABr: 4 CTAB: 7000 H2O. The synthesis process begins by dissolving NaOH in water and slowly adding CFAE at a temperature of 80-90°C. Subsequently, TPABr and CTAB are poured in alternately, with each addition spaced 10 minutes apart during stirring. The mixture is stirred until a white colloidal solution is formed. The mixture is then aged for 6, 12, 24 hours, and without aging. After aging, the mixture is transferred to an autoclave for the hydrothermal process and crystallization for 10, 24, 48, 72, and 120 hours at 150°C. The crystals obtained after hydrothermal process are washed to neutral pH, centrifuged at 3500 rpm for 20 minutes, dried at 120°C, and calcinated at 550°C for 6 hours [24, 25].

2.5 Characterization

The CFAP and CFAE products were characterized using X-ray fluorescence (XRF) to ascertain the elemental composition. The synthesized zeolite underwent analysis through Fourier Transform Infrared (FTIR) and X-ray diffraction (XRD). FTIR analysis, performed with a PerkinElmer Spectrum IR 10.7.2, was employed to confirm the successful formation of zeolite. The interpretation of functional groups within the 400-4000 cm^{-1} wavelength range validated zeolite formation. XRD analysis, conducted on a Bruker-binary V4 instrument using Cu *K-a* radiations at a scanning rate of 1°/minute (10 mA, 30 kV), provided insights into crystalline properties. The analysis spanned a 2θ range of 5°-80°, enabling the identification of crystal phases and mineral types, referencing databases such as the Inorganic Crystal Structure Database (ICSD), Crystallography Open Database (COD), and International Zeolites Association (IZA). Additionally, XRD analysis facilitated the determination of crystallinity and the average crystal diameter of the synthesized zeolite, utilizing the Debye-Scherrer equation

3.0 RESULT AND DISCUSSION

3.1 Characterization of CFAE

The XRF characterization in Table 1 reveals that CFAP contains four dominant compounds: SiO_2 (30.8462%), Fe_2O_3 (19.5270%), Al_2O_3 (16.7669%), and CaO (16.7443%). Additionally, minor compounds such as MgO (7.8544%) and SO3 (4.3685%) are present, with other compounds accounting for less than 1%. Based on the SiO_2, Al_2O_3, and Fe_2O_3 content in CFAP, it is evident that the fly ash originates from the combustion of bituminous coal [2].

Furthermore, in CFAE, two dominant compounds, silica, and alumina, confirm the success of the extraction process. The silica extract shows a remarkable increase of 73.16%, from 30.862% to 53.42%, and alumina exhibits a significant increase of 150%, from 16.8669% to 42.04%, compared to the pre-extraction percentages. There is a decrease in other dominant compounds, such as Fe_2O_3 (0.43%) and CaO (0.29%), the disappearance of MgO and SO_3, and other compounds below 0.1%. Moreover, some minor compounds show an increase, including P_2O_5 (1.76%) and K_2O (1.48%).

This research outperforms the alumina and silica extraction from CFA conducted by Missegue and colleagues [26], showing a more substantial increase of approximately 10% for SiO_2 and less than 10% for Al_2O_3. This study also reduces impurities exceeding 1%, such as Fe_2O_3 and CaO, to less than 0.5%.

Table 1 XRF analysis of materials

Compounds	CFAP (%)	CFAE (%)
SiO_2	30.8462	53.42
Al_2O_3	16.7669	42.04
Fe_2O_3	19.5270	0.43
CaO	16.7443	0.29
MgO	7.8544	-
SO_3	4.3685	-
P_2O_5	0.6530	1.76
Cl	0.098	0.03
K_2O	0.6761	1.48
Na_2O	0.2906	-
Sc_2O_3	0.0762	-
TiO_2	0.8094	-
V_2O_5	0.0366	0.11
Cr_2O_3	0.0392	0.02
MnO	0.7384	0.03
ZnO	0.0219	-
Rb_2O	0.0097	0.02
SrO	0.3518	0.05
ZrO_2	0.0436	-
NiO	0.0127	-
Y_2O_2	0.0130	-
Ta_2O_5	0.0224	-

3.2 Effect of Crystallization Time on Zeolite Synthesized

Figure 1 shows the FT-IR spectra results for the crystallization time influence over 10, 24, 48, 72, and 120 hours. Upon analysis of the FT-IR spectra above, sharp absorptions with strong intensity are observed at wavenumbers 991.40 (10h), 990.76 (24h), 982.15 (48h), (72h), and 990.45 cm^{-1} (120h). In this range (950-1250 cm^{-1}), these absorptions are identified as the asymmetric internal stretching vibrations of the T-O-T bonds in the tetrahedral building units TO_4 (T=Si/Al) throughout the zeolite framework [27, 28].

The absorption band vibrations within the 950-1250 cm^{-1} range are highly sensitive to changes in the Si/Al molar ratio. Therefore, variations in the distributed molar ratio within the zeolite framework structure will shift the direction of the resulting vibrations. The detection of vibrations at the wavenumber 983 cm^{-1} indicates the presence of a Sodalite (SOD) or Gismondine (GIS) framework structure in the synthesized zeolite [29].

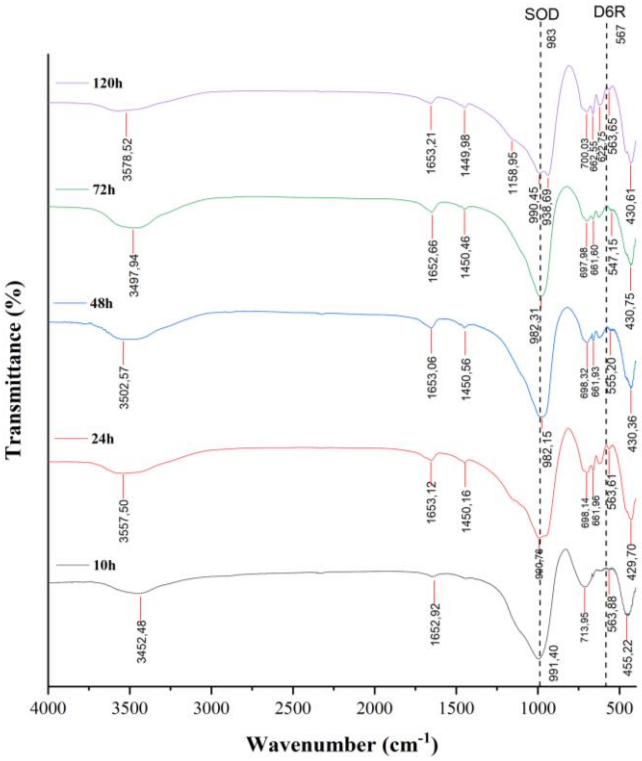

Figure 1 Spectra FT-IR of zeolites synthesized at various crystallization time

Specific peaks with sharp absorption and sufficiently strong intensity are also detected within the range of 650-720 cm^{-1} at wavenumbers 713.95 (10h), 661.96; 698.14 (24h), 661.93; 698.32 (48h), 661.90; 697.98 (72h), and 662.55; 700.03 cm^{-1} (120h). Within this range, these absorptions are identified as internal stretching vibrations of symmetric T-O-T bonds in the tetrahedral building units TO_4 [27]. Furthermore, sharp absorptions with sufficiently strong intensity are also detected within the range of 420-500 cm^{-1} at wavenumbers 455.22 (10h), 429.70 (24h), 430.36 (48h), 430.76 (72 h), and 430.61 (120h). These specific peaks are identified as vibrations of bending T-O bond [30, 31].

Within the range of 500-650 cm^{-1}, there is a weak intensity peak at wavenumbers 563.88 (10h), 563.61 (24h), 550.20 (48h), 547.14 (72h), and 563.65 cm^{-1} (120h). This specific peak represents the vibration of external T-O bonds in the zeolite building unit, referring to the 4 or 6-membered ring units (D4R or D6R) [28, 31]. Additionally, absorptions with very weak intensity are detected in the range of 1400-1467 cm^{-1} at wavenumbers 1450.16 (24h), 1450.56 (48h), 1450.06 (72h), and 1449.98 cm^{-1} (120h). These specific absorptions represent vibrations of Na-T bonds in the zeolite framework [32].

In addition to absorptions in the fingerprint region (400-1500 cm^{-1}), weak absorptions are also detected in the main region. Within the range of 1646-1655 cm^{-1}, an absorption with weak intensity is detected at wavenumbers 1652.92 (10h), 1653.12 (24h), 1653.06 (48h), 1652.66 (72h), and 1653.21 cm^{-1} (120h). The absorption at this specific peak is identified as water molecules (H-O-H) trapped within the zeolite channels [28, 31]. Furthermore, absorptions with broad peaks and low intensity in the range of 3300-3600 cm^{-1} at wavenumbers 3452.48 (10h), 3557.5 (24h), 3502.57 (48h), 3497.34 (72h), and 3578.52 cm^{-1} (120 hours). These absorptions are identified as stretching vibrations of hydroxyl groups (-OH) from silanol groups (Si-OH) located at the ends of the zeolite framework [30, 32].

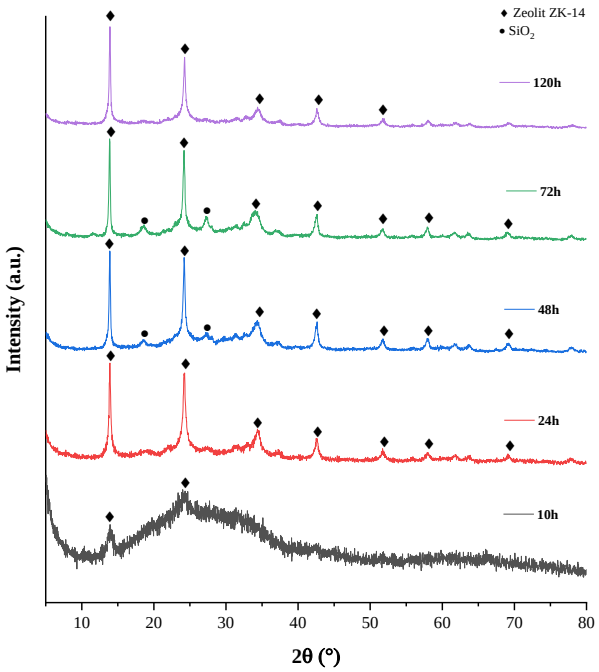

Figure 2 XRD patterns of zeolites synthesized at various crystallization time

Figure 2 shows the XRD pattern from the synthesis variations with crystallization times of 10, 24, 48, 72, and 120 hours at 2θ angles ranging from 5-80°. Based on Figure 2, it is evident that all diffractograms exhibit a high degree of similarity, indicating good crystallinity except for the diffractogram at the 10-hour crystallization time. In the 10-hour sample, only specific low-intensity peaks are observed at 2θ degrees of 13.9° and 24.19°. Furthermore, in the 24-hour sample, specific peaks with dominant intensity are observed at 2θ degrees of 13.9°, 24.19°, 34.4°, 42.68°, and weak intensity at 51.78°, 57.97°, and 69.18°.

A nearly identical diffractogram is also detected in the 48-hour sample. Specific peaks are identified at 2θ degrees of 13.9°, 24.20°, 34.40°, 42.63°, along with weak intensities at 18.5°, 27.45°, 51.78°, 57.76°, 58°, and 69.19°. In the 72-hour sample, specific peaks with dominant intensity are observed at 2θ degrees of 13.88°, 24.17°, 34.11°, 42.62°, along with weak intensities at 18.58°, 27.34°, 51.77°, 57.97°, and 69.10°. Finally, in the last sample of 120 hours, specific peaks

are obtained at 2θ degrees of 13.92°, 24.25°, 34.45°, 42.5°, along with weak intensities at 51.83° and 58.05°.

All zeolite products obtained at each crystallization time variation exhibit identical peaks at 13.9° and 24°, along with additional supporting peaks at 34° and 42°. Based on the analysis using X'pert Highscore Plus software, these highest peaks indicate that the formed zeolite phase is Zeolite ZK-14 with an SOD framework. This conclusion is supported by references such as ICSD 201587 and COD 96-152-9731. Additionally, there is another phase at peaks 18.5°, 27.45° (48h) and 18.58°, 27.34° (72h), identified as the SiO_2 phase. These findings are further validated by referencing the IZA database, as shown in Table 2.

Table 2 Interpretation of zeolites synthesized at crystallization time effect based on the IZA database

IZA Database		Crystallization time (Hours)									
SOD Framework		10h		24h		48h		72h		120h	
2θ°	r.i (%)	2θ°	r.i (%)	2θ°	r.i (%)	2θ°	r.i (%)	2θ°	r.i (%)	2θ°	r.i (%)
13.95	100	13.9	100	13.9	100	13.9	100	13.88	100	13.92	100
-	-	-	-	-	-	18.5	5.59	18.58	8.66	-	-
24.29	41.82	24.19	78.45	24.21	79.38	24.20	84.94	24.17	83.23	24.25	65.89
-	-	-	-	-	-	27.45	5.41	27.34	12.52	-	-
34.63	11.5	-	-	34.4	20.21	34.40	17.19	34.11	16.9	34.45	11.71
42.75	4.74	-	-	42.68	19.5	42.63	25.65	42.62	20.69	42.5	15.38
51.96	9.3	-	-	51.78	7.85	51.76	8.86	51.77	7.73	51.83	15.19
-	-	-	-	57.97	6.31	58	9.64	57.97	9.37	58.05	5.13
69.4	6.18	-	-	69.18	5.18	69.19	6.43	69.10	5.31	69.27	2.91

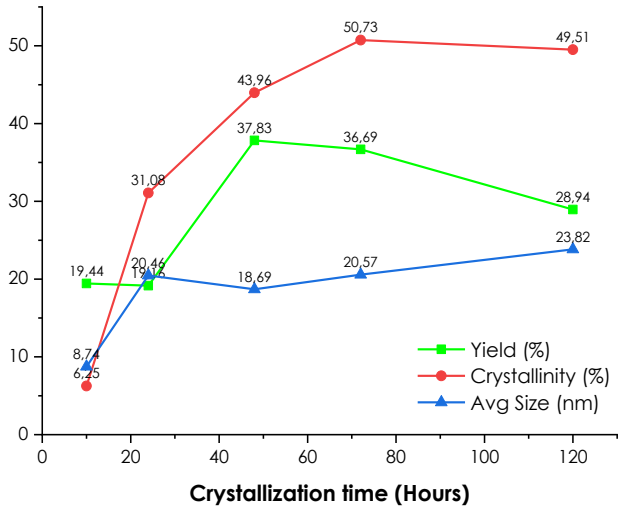

Figure 3 The effect of crystallization time on %yield, crystallinity, and average crystal diameter in zeolite synthesized

The variation in hydrothermal time during synthesis significantly impacts the %yield and crystallinity level of the produced zeolite. Based on the diffraction patterns in Figure 2, the zeolite synthesis with a 10-hour crystallization time has a crystallinity phase of only 6.25%, predominantly amorphous, with a %yield of 19.44%. Subsequently, at a 24-hour, the crystallinity increases significantly to 31.08% with a %yield of 19.16%. The crystallinity at 48, 72, and 120 hours increases to 43.96%, 50.73%, and 49.52%, respectively. The %yield also increases to 37.83% at 48 hours and 36.69% at 72 hours. However, there is a slight decrease in %yield at 120 hours, reaching 28.94%. The average crystal diameter sequentially obtained is 8.74, 20.46, 18.69, 20.57, and 23.82 nm.

Based on Figure 3, it can be observed that an increase in crystallization time during synthesis will also increase the crystallinity and average particle size of the zeolite product, as well as the %yield of zeolite obtained. From 24 to 72 hours, the product's crystallinity increases gradually and significantly, reaching its highest at 72 hours with a crystallinity of 50.73% and reaching the highest %yield at 48 hours, 37.83%. This is in line with the study conducted by Sun and colleagues [33], stating that increased crystallization time leads to more complete crystal growth. Although there is a slight decrease in crystallinity at 120 hours, it is not significant. There is a considerable increase in crystal diameter from 10 hours to 24 hours, but afterward, there is no significant change, and it tends to remain constant. The 120-hour crystallization time is the optimum duration for producing the largest average crystal size, 23.82 nm. The absence of further significant changes or improvements indicates that the synthesis conditions have reached the optimal state for each parameter.

The longer the crystallization time, the clearer the formation of zeolite crystals, with specific peaks appearing more prominently and forming a predominantly single zeolite phase with minimal amorphous content. This is because the growth of crystals during crystallization increases the density of the formed zeolite crystals, leading to the emergence of specific peaks with high intensity [34]. Figure 2 substantiates that the XRD pattern at 120 hours of crystallization time exhibits sharper, cleaner peaks and no visible amorphous phase compared to other diffraction patterns.

3.3 Effect of Aging Time on Zeolite Synthesized

The FT-IR spectra in Figure 4 represent the spectra of the synthesized zeolite under the influence of aging time variations for 0, 6, 12, and 24 hours.

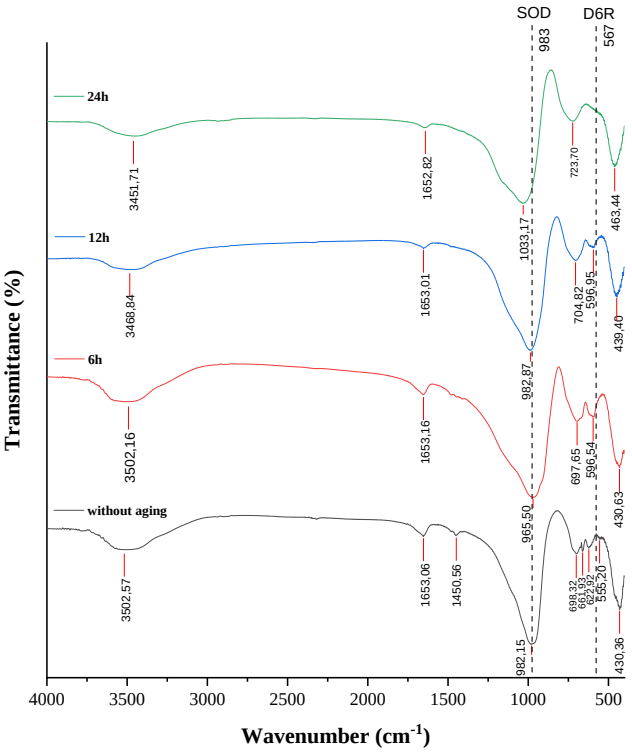

Figure 4 Spectra FT-IR of zeolites synthesized at various aging times

The generated FT-IR spectra appear almost identical and closely resemble the spectra produced under the influence of hydrothermal time at specific wavenumber ranges. In the wavenumber range of 950-1250 cm-1, there is a sharp absorption with strong intensity at 982.15 (without aging), 965.80 (6h), 982.87 (12h), and 1033.17 cm^{-1} (24h). This absorption is identified as the asymmetric stretching vibration of the T-O-T bonds in the tetrahedral building unit of the zeolite TO_4. These results closely resemble the spectra obtained for zeolite synthesis under the influence of hydrothermal time, and the absorption peak in the wavenumber range of 950-1250 cm^{-1} approximates the literature value of 983 cm^{-1}, which identifies it as a zeolite with a SOD or GIS framework [30].

Furthermore, in the wavenumber range of 650-720 cm^{-1}, there is a specific and sharp absorption with fairly strong intensity detected at 698.31 (without aging), 697.65 (6h), 704.82 (12h), and 723.70 cm^{-1} (24h). The absorption at this specific peak is indicated as the symmetric vibration of the T-O-T bonds in the tetrahedral building unit of the zeolite TO_4. Another sharp absorption with strong intensity is also detected in the wavenumber range of 420-500 cm^{-1}, specifically at 430.36 (without aging), 430.63 (6h), 439.40 (12h), and 463.44 cm^{-1} (24h). In this absorption, it can be identified as the bending vibration of the T-O bonds [27].

In the wavenumber range of 500-650 cm^{-1}, a reasonably sharp absorption with weak intensity is detected at 550.20 and 622.92 (without aging), 596.54 (6h), and 596.95 cm^{-1} (12h). However, no absorption is detected at the 24-hour aging period in this wavenumber range. Absorption in this wavenumber range indicates the vibration of double rings (D4R or D6R) in the zeolite structure [27]. According to the research by Jatarit and coworkers [35], the absorption detected at a wavenumber close to 567 cm^{-1} can be identified as the vibration of the double-ring unit 6 (D6R). Meanwhile, according to Król and coworkers [36], the absorption detected at a wavenumber close to 592 cm^{-1} indicates the vibration of the double-ring unit 4 (D4R). Subsequently, in the wavenumber range of 1400-1467 cm^{-1}, only a weak intensity absorption is detected under the condition without aging, specifically at 1450.56 cm^{-1}. This absorption indicates the vibration of the Na-T bond. Then, in the wavenumber range of 3300-3600 cm^{-1}, a broad and weak intensity absorption is detected at 3502.27 (without aging), 3502.16 (6h), 3488.84 (12h), and 3451.71 cm^{-1} (24h). The absorption in this wavenumber range represents the stretching vibration of the -OH groups in the silanol Si-OH [30, 32].

The specific peaks identified in the synthesis results for various aging times are almost identical to those obtained for various hydrothermal times. Detecting particular peaks in the fingerprint region, namely in the ranges of 950-1250, 650-720, and 500-650 cm^{-1}, confirms the formation of the zeolite framework structure in the synthesis results. The consistency between the zeolite synthesis results under hydrothermal and aging conditions indicates the production of zeolites with a SOD framework structure in both cases.

Table 3 Interpretation of zeolites synthesized at aging time effect based on the IZA database

IZA Database		Aging time (hours)							
SOD Framework		0h		6h		12h		24h	
2θ°	r.i (%)	2θ°	r.i (%)	2θ°	r.i (%)	2θ°	r.i (%)	2θ°	r.i (%)
13.95	100	13.9	100	13.43 13.88	76.35 100	13.37	100	- -	- -
-	-	18.5	5.59	18.58	36.1	18.59	44.83	-	-
-	-	-	-	22.93	56.52	22.94	57.35	-	-
24.29	41.82	24.20	84.94	24.16	73.85	-	-	-	-
-	-	27.45	5.41	27.23	28.71	-	-	-	-
-	-	-	-	29.60	36.52	29.55	58	-	-
34.63	11.5	34.40	17.19	-	-	-	-	-	-
42.75	4.74	42.63	25.65	42.55	21.82	-	-	-	-

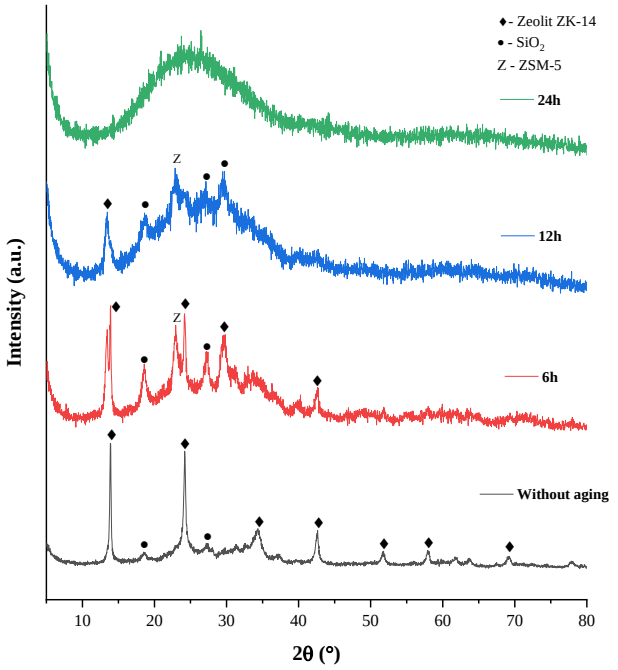

Figure 5 XRD patterns of zeolites synthesized at various aging times

Figure 5 shows the XRD patterns of all samples with varying aging times, namely 0, 6, 12, and 24 hours, at 2θ angles in the range of 5-80°. The zeolite synthesis product, without aging, produces a diffractogram with excellent crystallinity and minimal amorphous phase. Dominant peaks with strong intensity are observed at 2θ angles of 13.9°, 24.20°, 34.40°, 42.63°, along with weak intensity peaks at 18.5°, 27.45°, 51.76°, and 69.19°. Similarly, nearly identical peaks are detected in the synthesis results with a 6-hour aging time, with dominant peaks at 2θ angles of 13.88°, 18.58°, 22.93°, 24.16°, 27.23°, 29.60°, and 42.55°, exhibiting fairly strong intensity. However, the diffractogram obtained after 12 hours of aging produces less satisfactory results and exhibits an amorphous phase. Nevertheless, some weak intensity peaks are detected at 2θ angles of 13.37°, 18.59°, 22.94°, and 29.55°. In contrast to other diffractograms, the diffractogram at a 24-hour aging time does not yield specific peaks and maintains an amorphous phase. This indicates the presence of incomplete aluminosilicate precursors in the crystallization stage.

Based on the analysis results using X'pert Highscore Plus software, the diffraction pattern of the sample without aging is identified as Zeolite ZK-14 with a SOD framework. This interpretation is supported by the ICSD 201587 and COD 96-152-9731 as reference databases. The IZA database further substantiates this finding in Table 3.

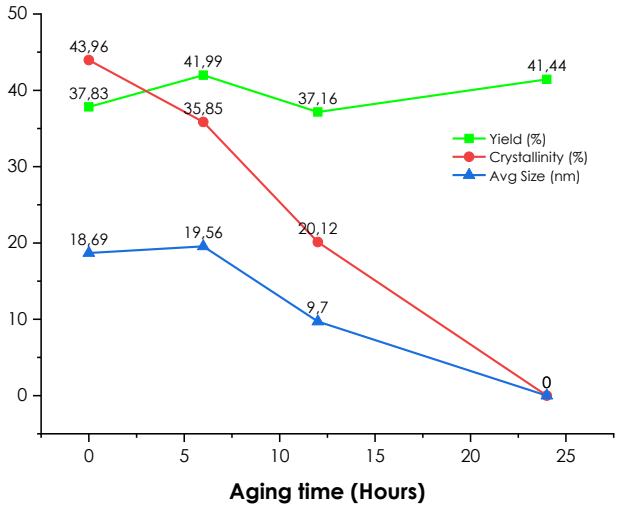

Figure 6 The effect of aging time on %yield, crystallinity, and average crystal diameter in zeolite synthesized

The difference in aging time during the synthesis process significantly influences the crystallinity of the zeolite product. Still, it does not have a pronounced effect on the percentage of the product (%yield) generated. The synthesis process without aging with a hydrothermal time of 24 hours yields a good %yield and crystallinity, namely 37.83% and 43.96%, respectively. Under the same conditions with a 6-hour aging time, the %yield is 41.99%, and the crystallinity is

35.85%. Subsequently, at 12 hours of aging, the %yield is 37.16%, and the crystallinity decreases to 20.12%. Meanwhile, with a 24-hour aging time, the %yield is 41.44%, and no crystalline phase is detected.

Figure 6 shows that under the same synthesis conditions (48 hours of hydrothermal time, T=150°C) with different aging times, the %yield of the resulting product does not significantly impact. However, it significantly influences crystallinity and the average crystal diameter. The longer the aging time under the same hydrothermal conditions, the lower the crystallinity and average crystal diameter.

This is supported by the diffraction patterns in Figure 5, indicating that a longer aging time results in an increased amorphous phase and a decrease in the specific peaks detected from crystals. The formation of a zeolite framework structure occurs when nucleation takes place in the gel during aging. The crystal growth rate will decrease during aging, and the nucleation rate will increase to form the zeolite framework [37]. In addition to reduced crystallinity, the crystal diameter does not tend to increase with longer aging times. The growth of crystallinity and crystal diameter will always be directly proportional, as both are influenced by the same factor: the crystal growth rate.

If not supported by an optimum crystallization time, the formed crystals will have low crystallinity or may only create an amorphous phase [31]. This is evidenced by the diffraction pattern in Figure 5, which shows that the 24-hour aging time with a 48-hour crystallization time is insufficient to form a stable crystalline phase of zeolite. Moreover, the aging process is crucial as it determines the initial phase of the zeolite framework that will be formed [31].

4.0 CONCLUSION

Silica and Alumina, extracted from CFA, have been successfully used as the main materials for synthesizing zeolite. The composition obtained is 42.04% Al_2O_3 and 53.42% SiO_2, compared to the initial values of 16.76% Al_2O_3 and 30.84% SiO_2. Utilizing these materials, zeolite ZK-14 with a SOD framework structure has been successfully synthesized, as confirmed by FTIR and XRD analyses. The variation in hydrothermal and aging times significantly influences the resulting zeolite crystals. Longer crystallization times lead to increased %yield, crystallinity, and crystal diameter due to the influence of crystal growth rates during the crystallization process. However, prolonged aging times, without a corresponding increase in crystallization time, may decrease crystallinity and crystal diameter, tending to remain in the amorphous phase. This is attributed to the prolonged nucleation formation period, leading to numerous amorphous aluminosilicate ions forming.

Acknowledgement

This work was supported by the Community Services and Research Institute (LPPM), University of Jambi, through the DIPA-PNBP funding under the Outstanding Applied Scheme of the University for the Fiscal Year 2023, as specified in Research Contract Number: 8/UN21.11/PT.01.05/SPK/2023 dated April 17, 2023.

Conflicts of Interest

The author(s) declare(s) that there is no conflict of interest regarding the publication of this paper.

References

[1] Miricioiu, M. G. and Niculescu, V. C. 2020. Fly Ash, from Recycling to Potential Raw Material for Mesoporous Silica Synthesis. *Nanomaterials*. 10(3): 1–14. https://doi.org/10.3390/nano10030474.

[2] Luo, Y., Y. Wu, S. Ma, S. Zheng, Y. Zhang and P. K. Chu. 2021. Utilization of Coal Fly Ash in China: A Mini-review on Challenges and Future Directions. *Environmental Science and Pollution Research*. 28(15): 18727–18740. https://doi.org/10.1007/s11356-020-08864-4.

[3] Vilakazi, A.Q., S. Ndlovu, L. Chipise and A. Shemi. 2022. The Recycling of Coal Fly Ash: A Review on Sustainable Developments and Economic Considerations. *Sustainability (Switzerland)*. 14(4): 1–32. https://doi.org/10.3390/su14041958.

[4] Ndlovu, N. Z. N. 2016. Synthesis of Zeolite (ZSM-5 and Faujasite) and Geopolymer from South African Coal Fly Ash. MSc Dissertation. Department of Mechanical Engineering, Cape Peninsula University of Technology. https://doi.org/10.1061/(ASCE)EE.1943-7870.0001212.

[5] Zahro, A., S. Amalia, T. K. Adi and N. Aini. 2014. Sintesis dan Karakterisasi Zeolit Y dari Abu Ampas Tebu Variasi Rasio Molar SiO_2/Al_2O_3 dengan Metode Sol Gel Hidrotermal. *Alchemy*. 3(2): 108–117. https://doi.org/10.18860/al.v0i1.2912.

[6] Chen, X., R. Jiang, Y. Gao, Z. Zhou, and X. Wang. 2021. Synthesis of Nano-ZSM-5 Zeolite Via a Dry Gel Conversion Crystallization Process and its Application in MTO Reaction. *CrystEngComm*. 23(15): 2793–2800. https://doi.org/10.1039/D1CE00162K.

[7] Kumaran, S., A. Kamari, A. A. Abdulrasool, S. T. S. Wong, J. Jumadi, S. N. M. Yusoff and S. Ishak. 2019. Synthesis, Characterisation and Mechanism of Novel Ca-ZSM-5 Zeolite Nanocomposite from Eggshell using Simple Co-Precipitation Method. *Journal of Physics: Conference Series*. 1397(1): 1–8. https://doi.org/10.1088/1742-6596/1397/1/012030.

[8] Ren, X., R. Qu, S. Liu, H. Zhao, W. Wu, H. Song, C. Zheng, X. Wu, and X. Gao. 2020. Synthesis of Zeolites from Coal Fly Ash for the Removal of Harmful Gaseous Pollutants: A Review. *Aerosol and Air Quality Research*. 20(5): 1127–1144. https://doi.org/10.4209/aaqr.2019.12.0651.

[9] Grewal, A. S., K. Karunesh, R. Sonika, and S. Bhardwaj. 2013. Microwave Assisted Synthesis: A Green Chemistry Approach. *International Research Journal of Pharmaceutical and Applied Sciences (IRJPAS)*. 3(5): 278–285.

[10] Mgbemere, H.E., I. C. Ekpa, G. I. Lawal, I. C. Ekpe and G. I. Lawal. 2017. Zeolite Synthesis, Characterisation and Application Areas: A Review. *International Research Journal Environmental Sciences*. 6(10): 45–59.

[11] Huang, D., X. Hu, C. Zhao, Y. Wu, J. Zhou, C. Liu, J. Yun, D. Chen, J. Dai, C. Cen and Z. Chen. 2020. Synthesis of Mesoporous ZSM-5 Zeolite and its Adsorption Properties for VOCs. *IOP Conference Series Earth Environmental Sciences*. 514(5): 1–7. https://doi.org/10.1088/1755-1315/514/5/052008.

[12] Feng, R., K. Chen, X. Yan, X. Hu, Y. Zhang and J. Wu. 2019. Synthesis of ZSM-5 Zeolite Using Coal Fly Ash as an Additive for the Methanol to Propylene (MTP) Reaction. *Catalysts*, 9(788): 1–13. https://doi.org/10.3390/catal9100788.

[13] Krisnandi, Y.K., F. M. Yanti and S. D. D. Murti. 2017. Synthesis of ZSM-5 Zeolite from Coal Fly Ash and Rice Husk: Characterization and Application for Partial Oxidation of Methane to Methanol. *IOP Conf. Series: Materials Science and Engineering*. 188(1): 1–6. https://doi.org/10.1088/1757-899X/188/1/012031.

[14] Adeleye, A.T., K. I. John, P. G. Adeleye, A. A. Akande and O. O. Banjoko. 2021. One-Dimensional Titanate Nanotube Materials: Heterogeneous Solid Catalysts for Sustainable Synthesis of Biofuel Precursors/Value-Added Chemicals - A Review. *Journal of Material Sciences*. 56(33): 18391–18416. https://doi.org/10.1007/s10853-021-06473-1.

[15] Jha, B., and D. N. Singh. 2016. *Fly Ash Zeolites: Innovations, Application and Directions*. Singapore: Springer. https://doi.org/10.1007/978-981-10-1404-8.

[16] Aldahri, T., J. Behin, H. Kazemian and S. Rohani. 2016. Synthesis of Zeolite Na-P from Coal Fly Ash by Thermo-sonochemical Treatment. *Fuel*. 182: 494–501. https://doi.org/10.1016/j.fuel.2016.06.019.

[17] Liu, Y., Q. Luo, G. Wang, X. Li and P. Na. 2018. Synthesis and Characterization of Zeolite from Coal Fly Ash. *Material Research Express*. 5(5): 1–10. https://doi.org/10.1088/2053-1591/aac3ae.

[18] Fitria, D., L. Marlinda, Rahmi, Y. M. Wulandari and M. Al-Muttaqii. 2021. The Effect of Aging Time on ZSM-5 Production from Siliceous Palm Oil Fly Ash. *ARPN Journal of Engineering and Applied Sciences*. 16(22): 2299–2304.

[19] Hamid, A., D. Prasetyo, T. E. Purbaningtias, F. Rohmah and I. D. Febriana. 2020. Pengaruh Tahap Kristalisasi pada Sintesis ZSM-5 Mesopori dari Kaolin Alam. *Indonesian Journal of Chemical Analysis*. 3(2): 40–49. https://doi.org/10.20885/ijca.vol3.iss2.art1.

[20] Hartanto, D., T. E. Purbaningtias, H. Fansuri and D. Prasetyoko. 2011. Karakterisasi Struktur Pori dan Morfologi ZSM-5 Mesopori yang Disintesis dengan Variasi Waktu Aging Pore Structure and Morphology Characterizations of Mesoporous ZSM-5 Synthesized at Various Aging Time. *Jurnal Ilmu Dasar*. 12(1): 80–90.

[21] Widayat, W., and A. N. Annisa. 2017. The Effect of Adding CTAB Template in ZSM-5 Synthesis. *Proceedings of the 3rd International Symposium on Applied Chemistry*, Jakarta, Indonesia. 1–8. https://doi.org/10.1063/1.5011918.

[22] Dhaneswara, D., J. F. Fatriansyah, F. W. Situmorang and A. N. Haqoh. 2020. Synthesis of Amorphous Silica from Rice Husk Ash: Comparing HCl and CH_3COOH Acidification Methods and Various Alkaline Concentrations, *International Journal of Technology*. 11(1): 200–208. https://doi.org/10.14716/ijtech.v11i1.3335.

[23] Azat, S., Z. Sartova, K. Bekseitova and K. Askaruly. 2019. Extraction of High-purity Silica from Rice Husk via Hydrochloric Acid Leaching Treatment. *Turkish Journal of Chemistry*. 43(5): 1258–1269. https://doi.org/10.3906/kim-1903-53.

[24] Wang, Q., S. Xu, J. Chen, Y. Wei, J. Li, D. Fan, Z. Yu, Y. Qi, Y. He, S. Xu, C. Yuan, Y. Zhou, J. Wang, M. Zhang, B. Su and Z. Liu. 2014. Synthesis of Mesoporous ZSM-5 Catalysts using Different Mesogenous Templates and Their Application in Methanol Conversion For Enhanced Catalyst Lifespan. *RSC Advances*. 4(41): 21479–21491. https://doi.org/10.1039/C4RA02695K.

[25] Ediati, R., A. Mukminin and N. Widiastuti. 2017. Impregnation of Nickel on Mesoporous ZSM-5 Templated Carbons as Candidate Material for Hydrogen Storage, *Indonesian Journal of Chemistry*. 17(1): 30–36. https://doi.org/10.22146/ijc.23563.

[26] Missengue, R. N. M., P. Losch, N. M. Musyoka, B. Louis, P. Pale and L. F. Petrik. 2018. Conversion of South African Coal Fly Ash into High-purity ZSM-5 Zeolite without Additional Source of Silica or Alumina and Its Application as a Methanol-to-olefins Catalyst. *Catalysts*. 8(4): 1–14. https://doi.org/10.3390/catal8040124.

[27] Nyankson, E., J. K. Efavi, A. Yaya, G. Manu, K. Asare, J. Daafuor and R. Y. Abrokwah. 2018. Synthesis and Characterisation of Zeolite-A and Zn-Exchanged Zeolite-A Based on Natural Aluminosilicates and Their Potential Applications. *Cogent Engineering*. 5(1): 1–23. https://doi.org/10.1080/23311916.2018.1440480.

[28] Byrappa, K. and B. V. S. Kumar. 2007. Characterization of Zeolites by Infrared Spectroscopy. *Asian Journal of Chemistry*. 9(6): 4933–4935.

[29] Ma, Y. K., S. Rigolet, L. Michelin, J. L. Paillaud, S. Mintova, F. Khoerunnisa, T. J. Daou and N. P. Ng. 2021. Facile and Fast Determination of Si/Al Ratio of Zeolites Using FTIR Spectroscopy Technique. *Microporous and Mesoporous Materials*. 311(110683): 1–4. https://doi.org/10.1016/j.micromeso.2020.110683.

[30] Li, C., X. Li, Q. Zhang, L. Li and S. Wang. 2021. The Alkaline Fusion-Hydrothermal Synthesis of Blast Furnace Slag-Based Zeolite (BFSZ): Effect of Crystallization Time. *Minerals*, 11(12): 1–11. https://doi.org/10.3390/min11121314.

[31] Nguyen, D. K., V. P. Dinh, N. T. Dang, D. T. Khan, N. T. Hung and N. H. T. Tran. 2023. Effects of Aging and Hydrothermal Treatment on the Crystallization of ZSM-5 Zeolite Synthesis from Bentonite. *RSC Advances*. 13(30): 20565–20574. https://doi.org/10.1039/D3RA02552G.

[32] Abdul-Moneim, M., A. A. Abdelmoneim, A. A. Geies and S. O. Farghaly. 2018. Synthesis, Characterization of Analcime and Its Application in Water Treatment from Heavy Metal. *Assiut University Bulletin fo Environmental Researchers*, 21(1): 1–22. https://doi.org/10.21608/auber.2018.133197.

[33] Sun, B., Y. Kang, Q. Shi, M. Arowo, Y. Luo, G. Chu and H. Zou. 2019. Synthesis of ZSM-5 by Hydrothermal Method with Pre-mixing in a Stirred-tank Reactor. *Canadian Journal of Chemical Engineering*. 97(12): 3063–3073. https://doi.org/10.1002/cjce.23593.

[34] Ayodeji, A. A., H. F. Kofi, O. J. Oladele, O. A. Esther, O. S. Fayomi and U. C. Chisom. 2017. Effect of Crystallisation Time on the Synthesis of Zeolite y from Elefun Kaolinite Clay. *International Journal of Applied Engineering Research*. 12(21): 10981–10988.

[35] Jantarit, N., P. Tayraukham, N. Osakoo, K. Föttinger and Wittayakun. 2020. Formation of EMT/FAU Intergrowth and Nanosized SOD Zeolites from Synthesis Gel of Zeolite NaX Containing Ethanol. *Material Research Express*. 7(7): 1–10. https://doi.org/10.1002/cjce.23593.

[36] Król, M., W. Mozgawa, W. Jastrzbski and K. Barczyk. 2012. Application of IR Spectra in the Studies of Zeolites from D4R and D6R Structural Groups. *Microporous and Mesoporous Materials*. 156: 181–188. https://doi.org/10.1016/j.micromeso.2012.02.040.

[37] Yoo, Y. S., H. J. Ban, K. H. Cheon and J. L. Lee. 2009. The Effect of Aging on Synthesis of Zeolite at High Temperature. *Materials Science Forum*. 620–622, 225–228. https://doi.org/10.4028/www.scientific.net/MSF.620-622.225.